

中国激光

基于超表面光场调控的阵列局域空心光束研究

张希纯¹, 吕金光², 张崇³, 付文升¹, 赵鑫¹, 李卫岩¹, 张贺^{1*}

¹长春理工大学高功率半导体激光器国家重点实验室, 吉林 长春 130022;

²中国科学院长春光学精密机械与物理研究所应用光学国家重点实验室, 吉林 长春 130033;

³陆军驻长春地区第一军事代表室, 吉林 长春 130000

摘要 设计了一种能够产生阵列局域空心光束的超表面透镜。该透镜基于几何相位原理, 通过调整二氧化钛纳米单元的长宽比以及旋转角度能够实现对波前的精确控制。超表面在波长为 632.8 nm 的左旋圆偏振光照射下, 能够产生多个微米级的局域空心光束, 并且可以通过控制环形障碍物的尺寸来改变产生局域空心光束的数量。该超表面透镜也可以通过改变相对孔径值(RA)来控制局域空心光束的横向和纵向半峰全宽的尺寸, 进而产生所需尺寸的阵列局域空心光束。

关键词 物理光学; 局域空心光束; 超表面; 几何相位; 干涉

中图分类号 O436

文献标志码 A

doi: 10.3788/CJL202148.2105001

1 引言

局域空心光束是一种沿传播方向上的三维空间内具有封闭暗域的特殊空心光束, 此暗域是由高强度的光围绕而成的封闭区域^[1-2]。由于这种特殊的光场分布, 局域空心光束在光镊^[3]、激光导管^[4]和光学微操作^[5]等方面都有着广泛的应用, 尤其是将局域空心光束应用于光镊时, 它可以稳定地捕获和操纵微观粒子。另外, 在操作过程中, 局域空心光束具有非接触和无强光照射的优势, 所以可以维持粒子的活性, 现如今已成功应用于生物医学领域。在过去的几十年里, 人们提出了不同的方法来产生局域空心光束, 如环缝-透镜法^[6]、轴棱锥-透镜系统法^[7]、双光束干涉法^[8]、光学全息法^[9]和 π 相位板法^[10]等。

自 2016 年哈佛大学的 Cappasso 课题组^[11]提出几何相位(Pancharatnam-Berry phase, PB phase)超表面之后, 超表面的研究已经成为当今国际学术界的研究热点。几何相位超表面通常由亚波长尺寸的光栅、矩形或椭圆形的各向异性单元按照一定的排列规律组成, 通过将这些单元旋转一定的角度, 可

以局部改变入射光的相位, 以此来实现任意入射光和反射光的振幅、相位和偏振的任意操控^[12-16], 从而塑造光束的波前, 同时超表面可以实现任意的反射、折射、偏振控制、定向传播等光束操纵功能。因此, 这种光学器件有可能替代或改进传统的折射型和衍射型光学元件^[17-20], 其中一个重要的应用便是基于超表面的光学透镜。例如基于金属和电介质类型的超表面已经可以将光聚焦到近场或远场^[21-26], 在可见光或红外光波长范围内^[20, 27-28]其甚至可以达到消色差的效果^[29]。

本文设计了一种以二氧化硅(SiO₂)为基底、二氧化钛(TiO₂)纳米柱为单元的超表面透镜, 入射光场通过该透镜后产生的球面波和贝塞尔光束相互干涉^[30], 能够产生多个高强度并且内径为微米级的局域空心光束。相比于传统光学系统, 其系统简单、集成度高, 产生的局域空心光束横向内径尺寸以及纵向内径尺寸显著减小, 对微小尺寸的粒子捕获更加精准。

2 超表面设计原理

2.1 光学系统设计

图 1 给出超表面光学系统的示意图。用准直器

收稿日期: 2021-02-02; 修回日期: 2021-03-22; 录用日期: 2021-04-09

基金项目: 应用光学国家重点实验室开放基金(SKLA02020001A17)

通信作者: *zhanghe@cust.edu.cn

对 He-Ne 激光器的入射光束进行准直,光束经过起偏器产生线偏振光,再经过 $\lambda/4$ 波片产生左旋圆偏振光束($\lambda/4$ 波片的快轴夹角需与起偏器的偏振方

向成 45° 以产生左旋圆偏振光束)。该光束入射到超表面上产生阵列局域空心光束,最后用 CCD 摄像机观察光斑。

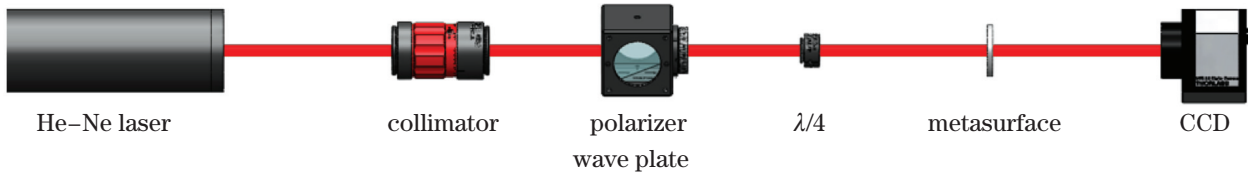


图 1 光学系统示意图

Fig. 1 Schematic diagram of optical system

2.2 超表面单元设计

当圆偏振光照射几何相位超表面时,其出射光会由左旋圆偏振光和右旋圆偏振光两部分组成,并且出射光中与入射光旋向相反的分量会携带几何相位延迟($2i\theta$),其中 θ 为纳米柱单元旋转角度, $i = \pm 1$ 分别代表左旋圆偏振(LCP)和右旋圆偏振(RCP)。

对于超表面的衬底,需要在工作波长下具有高透射率,从而降低损耗,提升器件的效率。对于构建超表面纳米结构的材料,需要同时具备高透射率和高折射率的特点。基于上述原因,本研究选择在二氧化硅(SiO_2)衬底上排列的二氧化钛

(TiO_2)纳米柱来构建具有相位调制能力的超表面。两种材料在 632.8 nm 波长下均具有高透射率,其中 TiO_2 满足在工作波长内折射率足够高、损耗率足够低两个条件。为了将超表面的工作波长设计为 632.8 nm,超表面纳米柱单元如图 2(a)所示,选取其长度 l 、宽度 w 和高度 h 分别为 377 nm、87 nm 和 600 nm,其偏振转换效率以及透射率均高于 85%。这里的偏振转换效率定义为:与入射光旋向相反的透射光强度与入射圆偏振光的强度之比。并且其几何相位延迟随着纳米柱的旋转可以覆盖 $0 \sim 2\pi$,这使其可以有效地控制波前,仿真结果如图 2(b)所示。

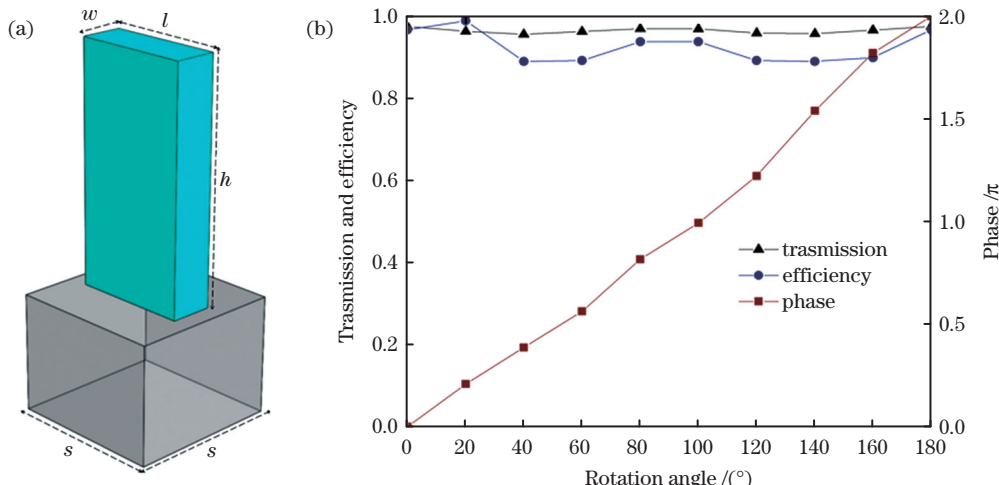


图 2 纳米柱单元示意图及其旋转角度与相关参数关系。(a)单个纳米柱单元示意图;(b)纳米柱单元旋转角度与透过率(三角形线)、偏振转化率(圆形线)、几何相位(方形线)的关系

Fig. 2 Schematic diagram of the nano-pillar unit and the relationship between its rotation angle and related parameters.

(a) Schematic diagram of a single nano-pillar unit; (b) relationship between the rotation angle of the nano-pillar unit and the transmittance(triangular line), polarization conversion efficiency(circular line), PB phase(square line)

2.3 超表面的相位分布

本文的超表面可以起到传统凸透镜的作用,也就是说,从超表面产生的波需在焦平面上干涉相长,进而形成焦点。因此在左旋圆偏振光入射下,超表面单元的双曲面相位分布可表示为^[11]

$$\varphi_1(x, y) = \frac{2\pi}{\lambda} [\sqrt{(x^2 + y^2) + f^2} - f], \quad (1)$$

其中, φ_1 代表相位延迟, λ 是入射波长, f 是给定的焦距, x 和 y 分别是纳米柱中心点的横向坐标和纵向坐标。基于几何相位原理可以通过旋转纳米单元

来实现相位延迟,超表面上的矩形纳米柱旋转角度的表达式为

$$\theta_1(x, y) = \frac{\pi}{\lambda} [\sqrt{(x^2 + y^2) + f^2} - f], \quad (2)$$

其中, θ_1 是矩形纳米柱旋转角度, 相位延迟 $\varphi_1(x, y)$ 与矩形柱单元旋转角度 $\theta_1(x, y)$ 的关系为 $\varphi_1(x, y) = 2\theta_1(x, y)$ 。对于起到轴棱锥作用的超表面, 其单元的锥面相位分布满足

$$\varphi_2(x, y) = \frac{2\pi}{\lambda} \sqrt{(x^2 + y^2)} \sin \alpha, \quad (3)$$

其中 α 表示出射光线与光轴夹角。

本文选取了半径 $R = 12 \mu\text{m}$ 、焦距 $f = 10 \mu\text{m}$ 的双曲面相位分布超表面[图 3(a)], 其纳米单元旋转角度由(2)式给出。如图 3(b)所示为该超表面沿光轴方向的透射场分布, 从中可以观察到光束聚焦现象。该光束焦平面处的光场分布如图 3(c)所示。

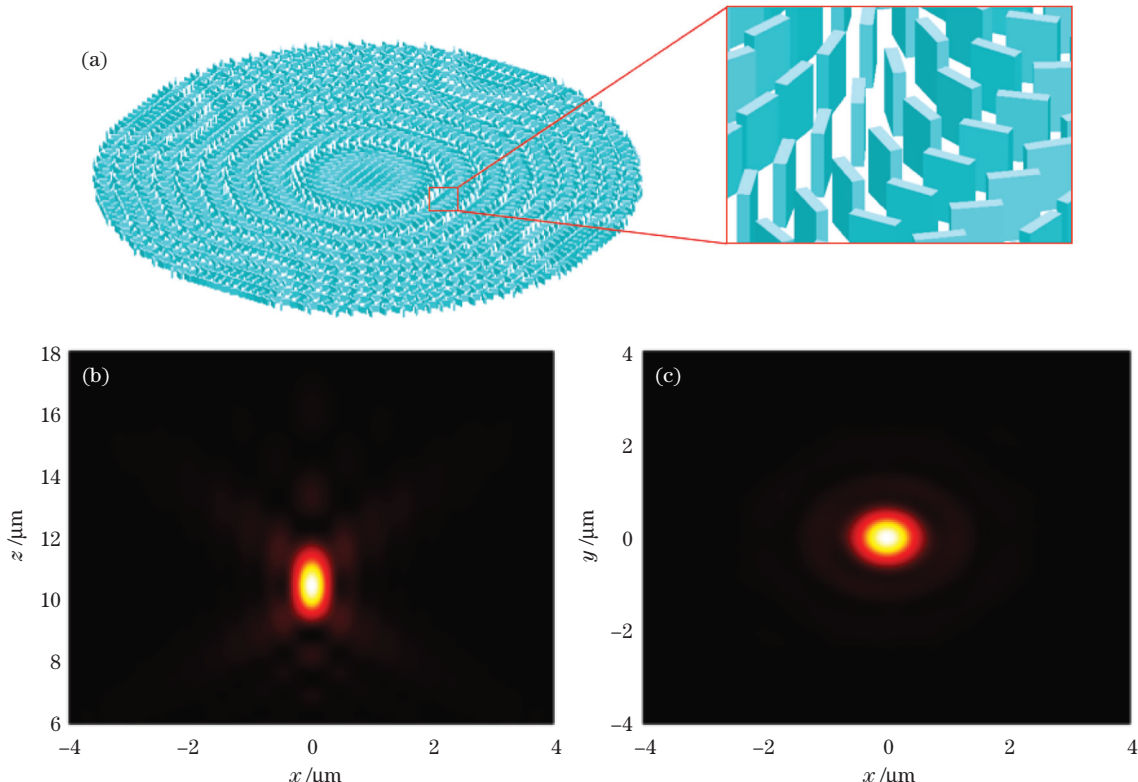


图 3 双曲面相位超表面示意图及光场分布。(a) 双曲面相位分布超表面三维示意图;(b) 超表面沿光束传播方向的光场分布;(c) 超表面沿光束传播方向的焦平面光场分布

Fig. 3 Schematic diagram of hyperbolic phase metasurface and light field distributions. (a) Three-dimensional schematic diagram of the hyperbolic phase distribution metasurface; (b) light field distribution of the metasurface along the beam propagation direction; (c) focal plane light field distribution of the metasurface along the beam propagation direction

在此基础上, 本文在该超表面基底上添加了一个半径 R_2 为 $6 \mu\text{m}$ 的不透光环形障碍物, 如图 4(a)所示, 障碍物将其分隔为内环、外环两部分。

如图 4(b)所示, 发现超表面外环部分产生了贝塞尔光束, 其产生原理如图 4(d)所示。图 4(d)为超表面相位与直径关系的截面图[相位分布如(1)式与(3)式所示], 其中虚线为双曲面相位分布, 实线为锥面相位分布。外环半径取 $R_3 = 2 \mu\text{m}$ 时, 可以发现如图 4(d)插图所示, 双曲面的相位在 $10 \sim 12 \mu\text{m}$ 处(外环部分)随半径改变呈线性变化, 形成锥面相位分布。由于产生贝塞尔光的超表面为锥面相位分

布[(3)式], 因此外环部分产生了贝塞尔光。图 4(c)为贝塞尔光束焦平面处的光场分布。

如图 5(a)所示为加上环形障碍物的超表面二维示意图。图 5(b)和图 5(c)所示分别为球面波、贝塞尔光沿光轴方向光场分布的示意图。超表面内环部分产生的球面波与外环部分产生的贝塞尔光相干叠加, 并在两光束相干叠加区域形成多个高强度的局域空心光束。如图 5(d)可见, 产生了 4 个完整的局域空心光束, 本研究将其分别标记为 1、2、3、4 号。图 5(e)~(g)分别为图 5(b)~(d)的线型分布示意图。

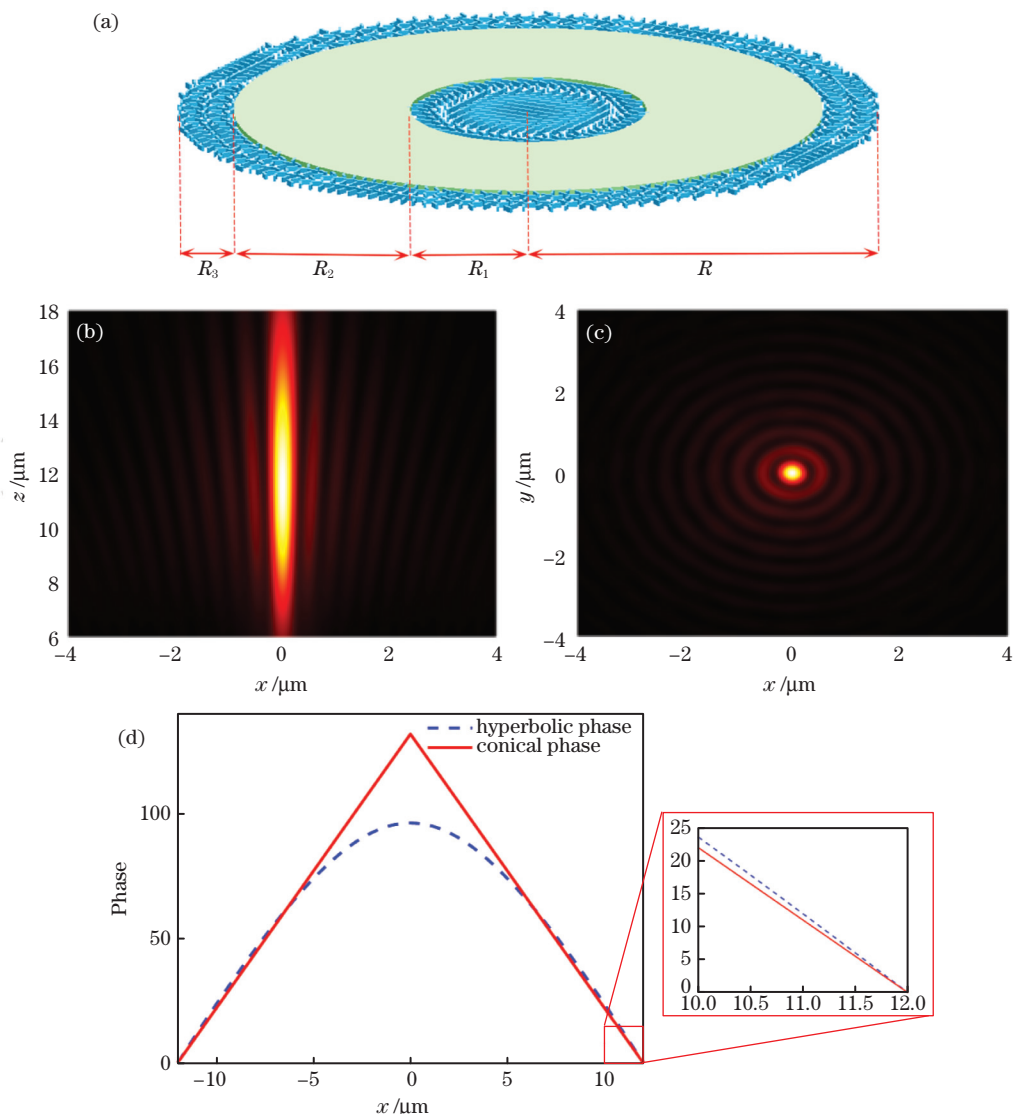


图4 加上环形障碍物后的超表面示意图、光场分布及相位曲线。(a)加上环形障碍物的超表面三维示意图;(b)超表面外环部分(半径为 R_3)沿光束传播方向光场分布;(c)图4(b)的焦平面光场分布;(d)双曲面相位与锥面相位对比图,虚线为双曲面相位分布,实线为锥面相位分布,插图为两种相位分布在半径 $10\sim12\mu\text{m}$ 时的放大图

Fig. 4 Schematic diagram, light field distribution and phase curves of the metasurface with an annular obstacle added.
 (a) A three-dimensional schematic diagram of the metasurface with the annular obstacle added; (b) optical field distribution of the outer ring part of the metasurface (radius R_3) along the beam propagation direction; (c) focal plane light field distribution of Fig. 4 (b); (d) hyperbolic phase and conical phase comparison chart, where the blue dotted line is the hyperbolic phase distribution, the solid line is the conical phase distribution, and the inset is an enlarged view of the two phase distributions in a radius of $10\sim12\mu\text{m}$

3 分析与讨论

3.1 局域空心光束光场分布

本文设计了一个半径为 $12\mu\text{m}$ 的超表面,采用左旋圆偏振光入射,焦距设计为 $10\mu\text{m}$ 。经过仿真计算,得到光束传播方向的光场分布如图6(a)所示,阵列局域空心光束在传播距离分别为 $9.45\mu\text{m}$ 、 $11.54\mu\text{m}$ (2、3号局域空心光束的焦平面处)的截面

光强如图6(b)和图6(c)所示。选择这两个局域空心光束,测得两个局域空心光束的横向半峰全宽(FWHM)分别为 $0.47\mu\text{m}$ 、 $0.61\mu\text{m}$,纵向半峰全宽分别为 $0.9\mu\text{m}$ 、 $1.2\mu\text{m}$ [如图6(d)~(f)所示],这里的横向和径向半峰全宽分别定义为:单个局域空心光束分别沿 x 和 z 方向光场最大强度一半处两点之间的距离。

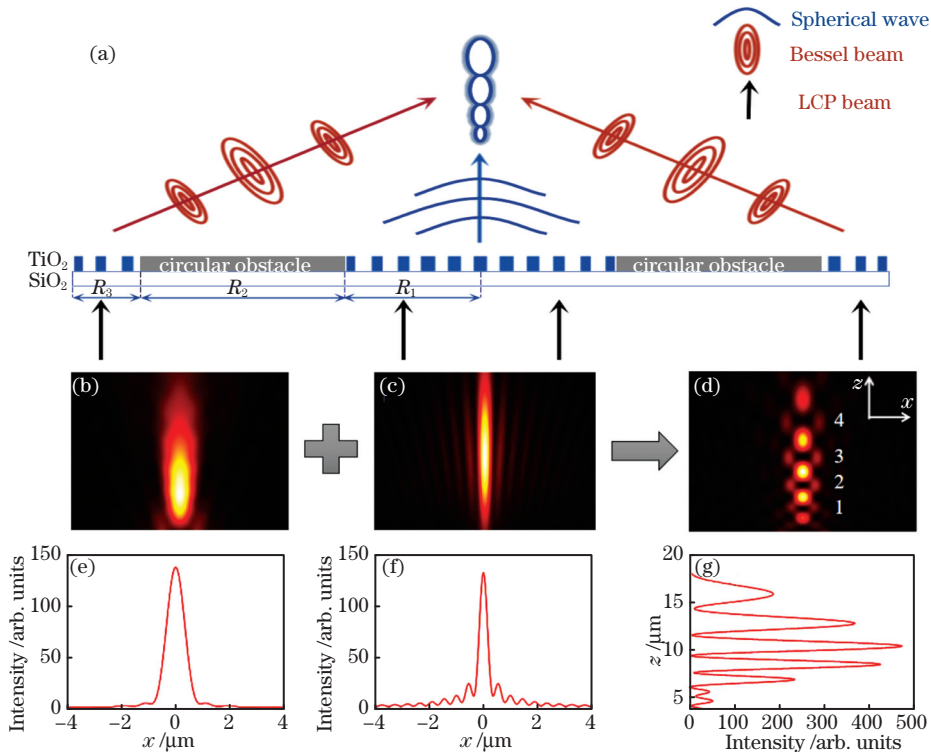


图5 环形障碍物超表面示意图、光场分布和线性分布。(a)加上环形障碍物的超表面二维示意图;(b)内环部分产生的球面波的光场分布;(c)外环部分产生的贝塞尔光的光场分布;(d)阵列局域空心光束的光场分布;(e)球面波图5(b)的线型分布;(f)贝塞尔光图5(c)的线型分布;(g)阵列局域空心光束图5(d)的线型分布

Fig. 5 Schematic diagram, light field distribution and linear distribution of the metasurface with ring-shaped obstacle added.
(a) A two-dimensional schematic diagram of the metasurface with the annular obstacle added; (b) optical field distribution of the spherical wave generated by the inner ring; (c) optical field distribution of the Bessel light generated by the outer ring; (d) optical field distribution of the array local hollow beam; (e) linear distribution of spherical wave in Fig. 5(b); (f) linear distribution of Bessel light in Fig. 5(c); (g) linear distribution of the multiple hollow beam in Fig. 5(d)

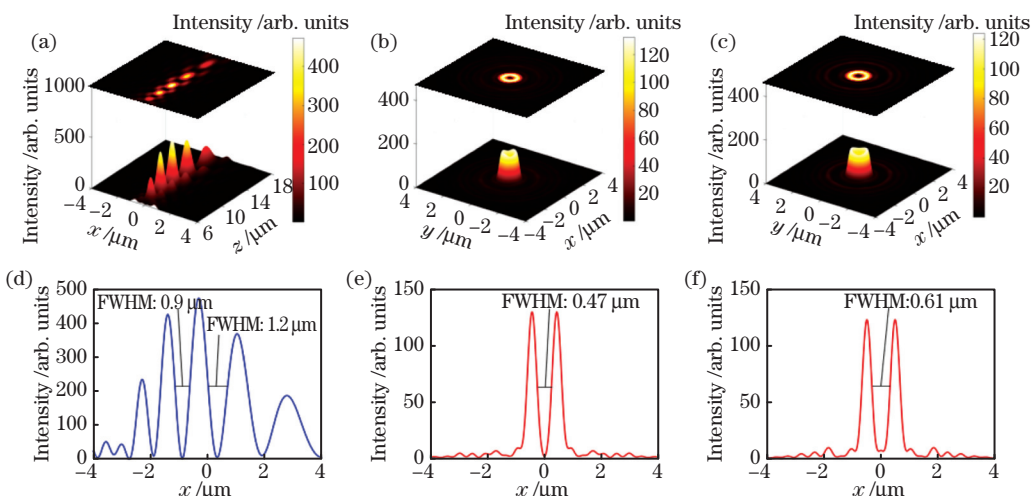


图6 阵列局域空心光束光场图及线型图。(a)阵列局域空心光束光束沿传播方向的光场分布;(b)(c)9.45 \$\mu\text{m}\$、11.54 \$\mu\text{m}\$处的光场分布;(d)图6(a)的线型分布,其中两个局域空心光束的纵向FWHM分别为0.9 \$\mu\text{m}\$、1.2 \$\mu\text{m}\$。(e)(f)图6(b)~(c)的线型分布,它们的横向FWHM分别为0.47 \$\mu\text{m}\$、0.61 \$\mu\text{m}\$

Fig. 6 Multiple bottle beam light field diagram and line type diagram. (a) Optical field distribution in the beam propagation direction of the multiple bottle beam; (b) (c) optical field distribution at 9.45 \$\mu\text{m}\$ and 11.54 \$\mu\text{m}\$; (d) linear distribution of Fig. 6(a), in which the longitudinal FWHM of the two hollow beams are 0.9 \$\mu\text{m}\$ and 1.2 \$\mu\text{m}\$, respectively; (e)(f) linear distribution of Fig. 6(b) and Fig. 6(c), and their transverse FWHM are 0.47 \$\mu\text{m}\$ and 0.61 \$\mu\text{m}\$, respectively

3.2 不同相对孔径值对局域空心光束光场的影响

当局域空心光束作为光镊去捕获不同类型的粒子时,为了实现更好的捕获效果,需要其尺寸是可调节的。本文将超表面的相对孔径值(RA, φ_{RA})定义为超表面的直径 D 与焦距 f 的比值。我们发现阵列局域空心光束的内径尺寸与超表面的 RA 存在对应关系。当 R_2 为超表面半径一半且 $R_1 : R_3 = 2 : 1$ 时,超表面直径从左至右依次增大时对应的径向光场分布如图 7(a)所示,从中可以观察到局域空心光束的横向与纵向内径逐渐减小。

图 7(b)~(c)为 2 号局域空心光束横向、径向 FWHM 与 RA 的关系,以及其线性拟合。当 RA 的值从 2 变为 3.6 时,横向 FWHM 的值从 $0.57 \mu\text{m}$ 变为 $0.2 \mu\text{m}$,径向 FWHM 的值从 $1.1 \mu\text{m}$ 减小为 $0.64 \mu\text{m}$,FWHM 与 RA 基本呈线性关系。因此,如果需要捕获特定尺寸的微粒,可以选用特定的 RA 来设计超表面,进而产生所需尺寸的局域空心光束。

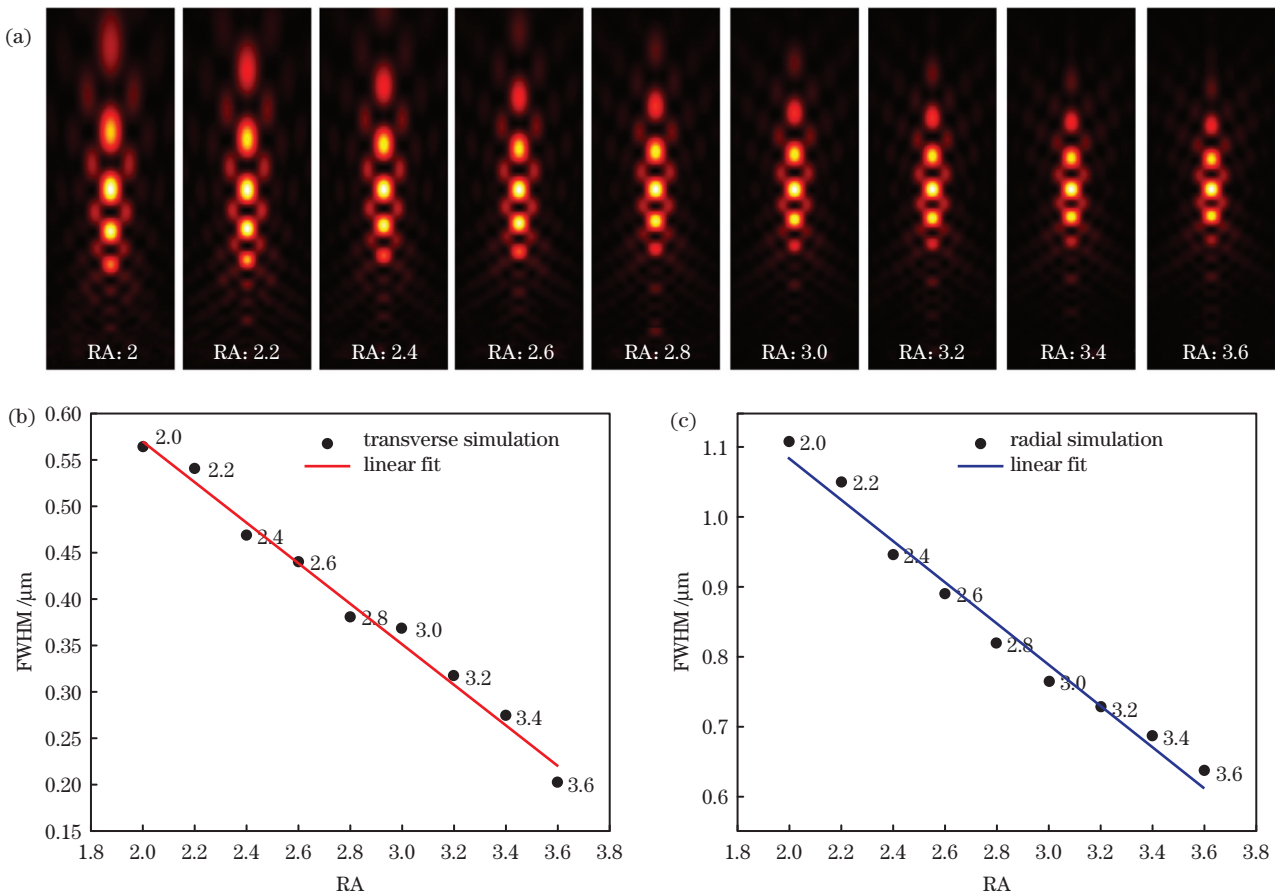


图 7 不同相对孔径值对局域空心光束光场的影响。(a)具有不同相对孔径值(RA)的阵列局域空心光束沿光束传播方向的二维光场分布图;(b)不同 RA 与横向 FWHM 的线性拟合;(c)不同 RA 与径向 FWHM 的线性拟合

Fig. 7 Influence of different relative aperture values on the light field of local hollow beam. (a) A two-dimensional optical field distribution diagram of an array local hollow beam with different RA along the beam propagation direction; (b) linear fit of different RA and transverse FWHM; (c)linear fitting of different RA and radial FWHM

3.3 不同孔径的环形光阑对局域空心光束光场的影响

当超表面上的环形障碍物尺寸不同时,产生的阵列局域空心光束个数是可以改变的。图 8(a)~(c)为超表面的径向光场分布图。本文的超表面半径取 $12 \mu\text{m}$,通过控制其外环尺寸 $R_3 = 2 \mu\text{m}$,改变环形障碍物的尺寸,使环形障碍物尺寸分别为 $R_2 = 5 \mu\text{m}$ 、 $6 \mu\text{m}$ 、 $7 \mu\text{m}$ [R_2 分别对应图 8(a)~(c)]。从图中不

难发现,局域空心光束的个数从左至右分别为 2、4、5 个。当超表面焦距不变时,可以通过增加超表面的半径来减小光场的尺寸,使光更加集中。因此,当产生聚焦光的内环面积逐渐减小[见图 8(a)~(c)]时,聚焦光束尺寸逐渐增大,聚焦光与贝塞尔光的干涉范围逐渐增加,进而使产生的局域空心光束数量依次增加。所以,可以通过控制超表面上环形障碍物的尺寸,改变产生的局域空心光束个数。

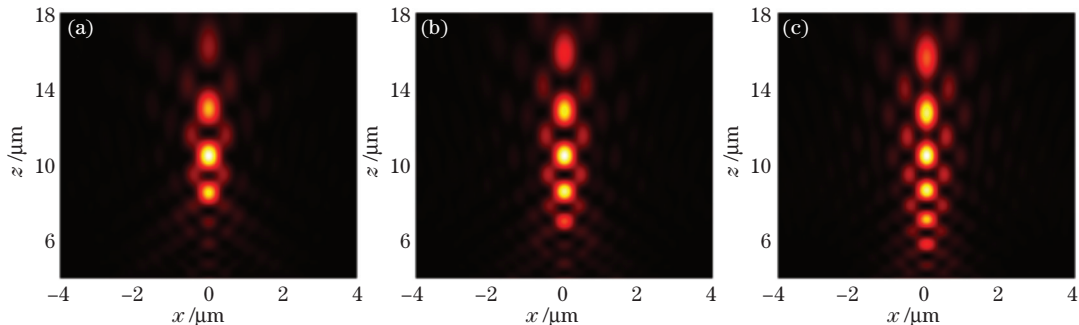


图8 环形障碍物孔径不同时超表面沿光束传播方向的二维光场分布图。(a) $R_2=5\text{ }\mu\text{m}$; (b) $R_2=6\text{ }\mu\text{m}$; (c) $R_2=7\text{ }\mu\text{m}$

Fig. 8 Two-dimensional light field distribution diagrams of a metasurface with different apertures of an annular obstacle along the beam propagation direction. (a) $R_2=5\text{ }\mu\text{m}$; (b) $R_2=6\text{ }\mu\text{m}$; (c) $R_2=7\text{ }\mu\text{m}$

4 结 论

利用几何相位超表面产生了多个微米级的局域空心光束,选取其中两个局域空心光束测得其横向 FWHM 分别为 $0.47\text{ }\mu\text{m}$ 、 $0.61\text{ }\mu\text{m}$,纵向 FWHM 分别为 $0.9\text{ }\mu\text{m}$ 、 $1.2\text{ }\mu\text{m}$ 。局域空心光束的横向 FWHM、纵向 FWHM 与超表面的相对孔径值(RA)呈反比,因此可以通过改变超表面的 RA(或 D/f)对阵列局域空心光束的空心区域大小进行调控,进而设计超表面透镜来捕获相应尺寸的微粒。同时该超表面透镜也可以通过控制环形障碍物的尺寸,改变产生阵列局域空心光束的个数。

与使用传统光学器件产生局域空心光束的常规方法相比,超表面更加轻巧、超薄、易于集成,并且本文产生的阵列局域空心光束尺寸显著减小,对微小粒子捕获更加精确,该阵列局域空心光束将会在超分辨率显微镜、超分辨率光刻、高密度数据存储、纳米粒子光学微操作和纳米光学制造等领域有所应用。

参 考 文 献

- [1] Arlt J, Padgett M J. Generation of a beam with a dark focus surrounded by regions of higher intensity: the optical bottle beam[J]. Optics Letters, 2000, 25 (4): 191-193.
- [2] Qiu P Z, Yu B B, Jing M, et al. Excitation of in-plane surface plasmon polariton bottle beams by multiple-incident-light illumination [J]. Applied Physics Express, 2018, 11(7): 072003.
- [3] Ashkin A, Dziedzic J M, Yamane T. Optical trapping and manipulation of single cells using infrared laser beams[J]. Nature, 1987, 330(6150): 769-771.
- [4] Snakard E P, Miller M, Berridge B, et al. Cooled-tip diode laser catheter for improved catheter ablation of ventricular tachycardia [J]. Journal of Investigative Surgery, 2001, 14(6): 357-366.
- [5] Andersson-Engels S, Andersen P E. Selected topics in biophotonics: photodynamic therapy and optical micromanipulation for biophotonics [J]. Journal of Biomedical Optics, 2010, 15(4): 041501.
- [6] Durnin J, Miceli J J, Eberly J H. Diffraction-free beams[J]. Physical Review Letters, 1987, 58(15): 1499-1501.
- [7] Wu F T, Lu W H, Ma B T. The beam propagation and transformation in axicon-lens system [J]. Acta Optica Sinica, 2009, 29(9): 2557-2560.
- [8] Isenhower L, Williams W, Dally A, et al. Atom trapping in an interferometrically generated bottle beam trap[J]. Optics Letters, 2009, 34(8): 1159-1161.
- [9] McGloin D, Spalding G, Melville H, et al. Applications of spatial light modulators in atom optics [J]. Optics Express, 2003, 11(2): 158-166.
- [10] Ozeri R, Khaykovich L, Davidson N. Long spin relaxation times in a single-beam blue-detuned optical trap[J]. Physical Review A, 1999, 59(3): R1750.
- [11] Khorasaninejad M, Chen W T, Devlin R C, et al. Metolenses at visible wavelengths: diffraction-limited focusing and subwavelength resolution imaging [J]. Science, 2016, 352(6290): 1190-1194.
- [12] Zheludev N I, Kivshar Y S. From metamaterials to metadevices[J]. Nature Materials, 2012, 11(11): 917-924.
- [13] Meinzer N, Barnes W L, Hooper I R. Plasmonic meta-atoms and metasurfaces[J]. Nature Photonics, 2014, 8(12): 889-898.
- [14] Yu N F, Capasso F. Flat optics with designer metasurfaces[J]. Nature Materials, 2014, 13(2): 139-150.

- [15] Arbabi A, Horie Y, Bagheri M, et al. Dielectric metasurfaces for complete control of phase and polarization with subwavelength spatial resolution and high transmission[J]. *Nature Nanotechnology*, 2015, 10(11): 937-943.
- [16] Kruk S, Hopkins B, Kravchenko I I, et al. Invited article: broadband highly efficient dielectric metadevices for polarization control[J]. *APL Photonics*, 2016, 1(3): 030801.
- [17] Fattal D, Li J J, Peng Z, et al. Flat dielectric grating reflectors with focusing abilities[J]. *Nature Photonics*, 2010, 4(7): 466-470.
- [18] Pfeiffer C, Grbic A. Metamaterial Huygens' surfaces: tailoring wave fronts with reflectionless sheets[J]. *Physical Review Letters*, 2013, 110(19): 197401.
- [19] Lin D, Fan P, Hasman E, et al. Dielectric gradient metasurface optical elements[J]. *Science*, 2014, 345 (6194): 298-302.
- [20] Decker M, Staude I, Falkner M, et al. High-efficiency dielectric Huygens' surfaces[J]. *Advanced Optical Materials*, 2015, 3(6): 813-820.
- [21] Yin L L, Vlasko-Vlasov V K, Pearson J, et al. Subwavelength focusing and guiding of surface plasmons[J]. *Nano Letters*, 2005, 5 (7): 1399-1402.
- [22] Liu Z W, Steele J M, Srituravanich W, et al. Focusing surface plasmons with a plasmonic lens[J]. *Nano Letters*, 2005, 5(9): 1726-1729.
- [23] Huang F M, Zheludev N, Chen Y F, et al. Focusing of light by a nanohole array [J]. *Applied Physics Letters*, 2007, 90(9): 091119.
- [24] Xiang M, Kuang D F, Gu P C, et al. Multi-wavelength multifocal metasurface with polarization multiplexing[J]. *Chinese Journal of Lasers*, 2020, 47 (11): 1113001.
- [25] Liang Y, Xu Y Y, Zou Y, et al. Design of achromatic polarization-insensitive metalens[J]. *Chinese Journal of Lasers*, 2021, 48(3): 0303001.
- [26] Luo Y, Wang W T, Zhao P J, et al. Dual-mode metasurface of polarization-specific focusing and keeping wavefront [J]. *Chinese Journal of Lasers*, 2020, 47(3): 0301007.
- [27] Lu F L, Sedgwick F G, Karagodsky V, et al. Planar high-numerical-aperture low-loss focusing reflectors and lenses using subwavelength high contrast gratings [J]. *Optics Express*, 2010, 18(12): 12606-12614.
- [28] Arbabi A, Horie Y, Ball A J, et al. Subwavelength-thick lenses with high numerical apertures and large efficiency based on high-contrast transmitarrays[J]. *Nature Communications*, 2015, 6: 7069.
- [29] Wang S, Wu P C, Su V C, et al. Broadband achromatic optical metasurface devices [J]. *Nature Communications*, 2017, 8(1): 187.
- [30] Cheng Z M, Wu F T, Fang X, et al. Multi-bottle beam generated by vaulted axicon[J]. *Acta Physica Sinica*, 2012, 61(21): 214201.
- 程治明, 吴逢铁, 方翔, 等. 圆顶轴棱锥产生多个局域空心光束[J]. *物理学报*, 2012, 61(21): 214201.

Multiple Bottle Beams Based on Metasurface Light Field Control

Zhang Xichun¹, Lü Jinguang², Zhang Chong³, Fu Wensheng¹,
Zhao Xin¹, Li Weiyan¹, Zhang He^{1*}

¹ State Key Laboratory of High Power Semiconductor Lasers, Changchun University of Science and Technology,
Changchun, Jilin 130022, China;

² State Key Laboratory of Applied Optics, Changchun Institute of Optics, Fine Mechanics and Physics,
Chinese Academy of Sciences, Changchun, Jilin 130033, China;

³ The First Military Representative Office of the Army in Changchun, Changchun, Jilin 130033, China

Abstract

Objective Recent studies have shown that the optical system that produces the bottle beam is gradually diversifying. However, most optical systems are more complex and the resulting bottle beams are larger in size. This article uses the metasurface to generate a bottle beam. The ultrasurface system is straightforward and well-integrated. The lateral and longitudinal inner diameters of the generated bottle beam are considerably reduced, and

the capture of tiny particles is more accurate. This has potential research and application value for multiparticle capture and precise capture.

Methods In this study, to generate multiple bottle beams, an opaque annular obstacle is added to the metasurface with the hyperbolic phase distribution (PB phase). The metasurface is constructed with titanium dioxide (TiO_2) nanopillars arranged on a silicon dioxide (SiO_2) substrate. To design the working wavelength of the nanopillars to 632.8 nm, the length, width, and height of the super surface nanopillars are designed to be 377, 87, and 600 nm, respectively. Moreover, by varying the relative aperture value (RA) of the metasurface, the lateral and longitudinal inner diameters of the bottle beam are altered. The number of bottle beams produced can be altered by changing the size of the annular obstacle on the metasurface.

Results and Discussions This article produced four micron-level bottle beams [Fig. 6(a)]. Further, by increasing the RA value of the metasurface, the lateral and longitudinal inner diameters of the bottle beams are reduced [Fig. 7(a)]. Thus, the RA value of the metasurface can be changed to alter the size of the generated light field. We select one of the bottle beams and observe that its transverse and radial full width at half maximum (FWHM) are roughly linear with RA [Fig. 7(b)–(c)]. In this paper, the number of bottle beams produced is changed by changing the size of the annular obstacle on the metasurface [Fig. 8(a)–(c)].

Conclusions The metasurface method used in this paper generates four bottle beams. Two of the bottle beams are selected. The measured FWHMs of the two bottle beams are 0.47 and 0.61 μm in the transverse direction, respectively, and 0.9 and 1.2 μm in the longitudinal direction. Simultaneously, this paper finds that by changing the RA value of the metasurface, the inner diameter of the multiple bottle beams is variable, and its transverse FWHM and radial FWHM are roughly linear with RA. Therefore, if particles with a specific size need to be captured, the metasurface with a specific RA can be designed to generate a bottle beam with the required size. This paper also found that the size of the outer ring that controls the annular obstacle remains unchanged, and when its size is changed, the number of the bottle beams is changed to 2, 4, and 5, respectively. The size of the multiple bottle beams produced in this paper is considerably reduced, and capturing tiny particles is more accurate, which is of great significance to the study of particle capture.

Key words physical optics; bottle beam; metasurface; Pancharatnam-Berry phase; interference

OCIS codes 160.3918; 350.3950; 050.6624